


# Chapter 4

## Low Flicker Noise Current-Folded Mixer



The chapter presents a current-folded mixer achieving low  $1/f$  noise for low power direct conversion receivers. Section 4.1 introduces the necessity of low  $1/f$  noise mixer and the design objects. The design considerations of  $1/f$  noise reduction is discussed in Section 4.2. The proposed mixer topology decouples the design tradeoffs between noise figure, conversion gain and third order intermodulation distortion and is described in detail in Section 4.3. The current-folded mixer with  $1/f$  noise minimized shows significant improvements and the comparisons with the conventional current-reused injection topology is presented in Section 4.4. Experimental results have revealed the advantages of the newly proposed topology are and will be described in Section 4.5.

### 4.1 Introduction

The performance of CMOS direct conversion receivers rely very much on mixer design since it might induce DC offset, even order distortion and  $1/f$  noise. The  $1/f$  noise issue is the worst design obstacle since CMOS devices are surface channel

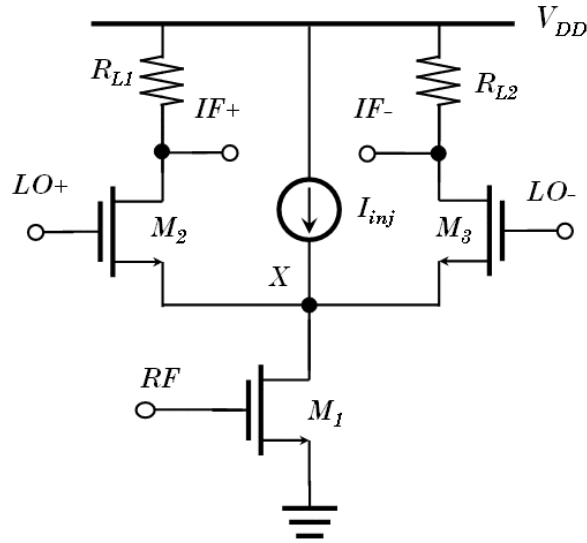


Figure 4.1: A single-balanced mixer with charge injection.

devices and have worse  $1/f$  noise compared with bipolar devices. The down converted received signal of a direct conversion receiver is located at baseband and easily corrupted by  $1/f$  noise. In addition, as the multi-carrier modulation becomes more popular in wireless standards, receivers are facing more strict requirements on linearity performance and the situation is getting more severe as the technology and power supply continuously scale down. Therefore minimizing  $1/f$  noise while achieve enough conversion gain and good linearity is essential and will be of great contribution to CMOS active mixers for direct conversion receivers. Gilbert-cell topology is the conventional CMOS active mixer that shows the significant design tradeoffs in conversion gain, noise figure and intermodulation distortions. The chapter presents a newly proposed mixer topology that exhibits low  $1/f$  noise while alleviates the design tradeoffs.

## 4.2 Design Considerations on 1/f Noise Reduction

The 1/f noise of a single-balanced Gilbert-cell mixer comes from the input stage and the switching stage through the mechanisms as reported in [40]. It is believed that the switching stage dominates the 1/f noise contribution at the mixer output. To minimize 1/f noise of the switching stage, the dimension of switching-pair devices can be made larger but this increases the noise contribution of in-direct mechanism of 1/f noise through parasitic capacitance at the common node of the source coupled switching pair.

If the output noise current of a mixer is modeled as an effective transconductance times input noise voltage source or  $i_{n,o} = G_{n,eff} \cdot v_{n,i}$ , the effective transconductances of 1/f noise and thermal noise in switching stage can be expressed as

$$G_{n,1/f,sw} = \frac{4I_{tail}}{ST_{LO}} \quad (4.1)$$

$$G_{n,thermal,sw} = \sqrt{\frac{2}{T_{LO}T_s}} \frac{2I_{tail}}{S} \quad (4.2)$$

where  $I_{tail}$  is the tail current biasing the switching stage,  $S$  is the slope of local oscillator (LO) waveform at zero crossing,  $T_{LO}$  is the LO period, and  $T_s$  is the duration at which both of the switching pair are conducting [40]. Therefore  $I_{tail}$  can be minimized to reduce both 1/f noise and thermal noise contributions of the switching stage. However,  $I_{tail}$  is also drawn by the input stage in Gilbert-cell topologies and minimizing it will degrade the conversion gain,

$$G_c = \frac{2}{\pi} g_m R_L \quad (4.3)$$

$$= \frac{2}{\pi} \cdot \frac{2I_{tail}}{V_{eff}} \cdot \frac{V_{eff}/2 + \varepsilon_{sat}L}{V_{eff} + \varepsilon_{sat}L} \cdot R_L \quad (4.4)$$

where  $V_{eff}$  is the transistor gate over-drive voltage ( $V_{GS} - V_t$ ) and  $\varepsilon_{sat}$  is the saturated

electric field, which takes into account velocity saturation of I-V characteristic of short-channel MOSFETs [41]. The degradation of conversion gain can be recovered by either increasing load resistance  $R_L$  or decreasing gate over-drive voltage  $V_{eff}$ , however, either case results in linearity degradation of Gilbert-cell mixers. This is a major tradeoff of Gilbert-cell mixers intended for direct conversion receivers.

To decouple the tradeoff, the tail current of switching stage and the current of input stage should be separated as suggested in [42]. The charge injection [43] and current-reused injection [44] mixers proposed prior to the above suggestion are tentative solutions to the design tradeoff as shown in Figure 4.1 and Figure 4.2. Both topologies are based on injecting a current  $I_{inj}$  to separate the biasing current of switching stage and that of input stage. The separation also decouples the design tradeoff in conversion gain and the input third-order intermodulation intercept point (IIP3) [43].

On the other hand, the common source nodes  $X$  of the switching stage in both topologies are tied to the drain nodes of the input stage, which leaks the input stage 1/f noise to the output through the mismatch of switching pair. The effective transconductance of the input-stage 1/f noise that leaks to the output can be given by

$$G_{n,1/f,os} = \frac{4g_{m1}v_{os}}{ST_{LO}}, \quad (4.5)$$

which is usually neglected in conventional Gilbert-cell mixers, since the offset voltage  $v_{os}$  is usually small [40]. However, the leakage is no longer negligible in current-injection mixers and the reason is addressed as follows. Noticing that  $I_{tail}$  in Eq. (4.1) means the current portion commutated by the switching pair. For Gilbert-cell mixers,  $I_{tail}$  equals to the current drawn by input stage. However, if current-injection topology is employed,  $I_{tail}$  means the residue current biasing the switching pair and is determined by the difference of input stage current and injected current, i.e.  $I_{tail} = I_{d1} - I_{inj}$ . In order to increase the conversion gain while keep the current consumption low,  $I_{d1}$  is usually made only slightly larger than  $I_{inj}$  and this

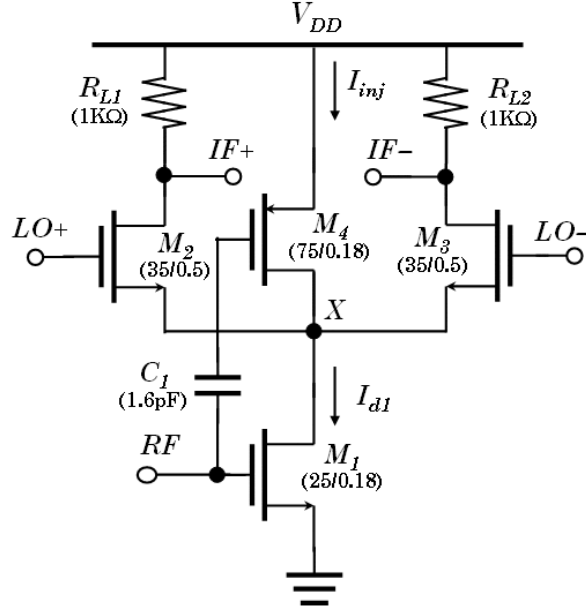


Figure 4.2: A single-balanced mixer with current-reused injection.

leads  $I_{tail}$  substantially small. Moreover, according to Eq. (4.1), to reduce the  $1/f$  noise voltage of the switching stage a smaller biasing current  $I_{tail}$  of switching stage is desirable. As a result, Eq. (4.5) and (4.1) are comparable, that is,  $I_{tail} \approx g_{m1}v_{os}$  and  $G_{n,1/f,os} \approx G_{n,1/f,sw}$ . Therefore, the contributions of  $1/f$  noise sources in switching stage and in input stage are similar and the latter one can not be neglected anymore. This is the side effect of current-injection mixers. To further reduce the  $1/f$  noise of input stage, a current-folded mixer is newly proposed.

### 4.3 The Proposed Current-Folded Topology

The proposed current-folded mixer is shown in Figure 4.3. The input stage consists of an NMOS and a PMOS as the V-I conversion. The input stage is AC coupled to switching stage with a MIM capacitor  $C_2$  to separate the V-I conversion and the switching stage. The tail current source of conventional current-folded architecture is replaced by a spiral inductor  $L_1$ . The inductor  $L_1$  acts as a current source for the

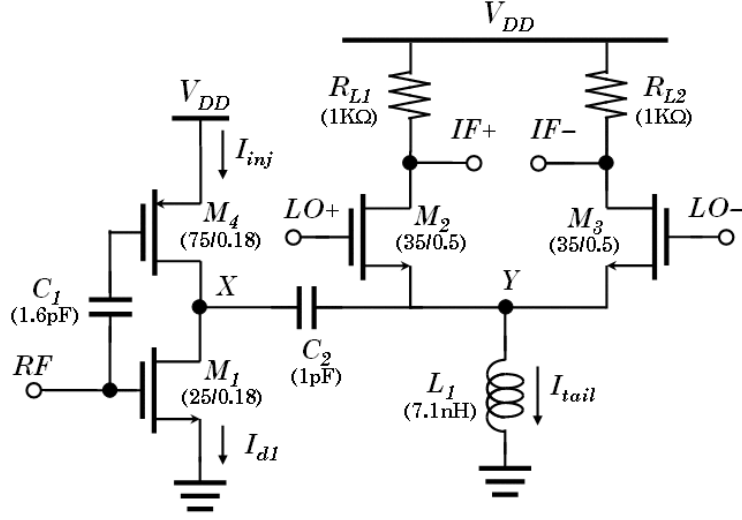


Figure 4.3: A single-balanced mixer with the proposed low-voltage current-folded topology.

desired signal while as a short circuit for the unwanted  $1/f$  noise. In addition,  $L_1$  also tunes out the parasitic capacitance of the switching pair and reduces  $1/f$  noise through indirect mechanism [40].

Figure 4.4 shows the equivalent circuit of the mixer. Impedance  $Z_c$  represents the capacitor  $C_2$  and the series parasitic resistor  $R_c$ . The quality factor of the MIM capacitor is quite high that  $R_c$  is negligible. In addition, the MIM capacitor has a metal layer as ground shielding and therefore the substrate loss can be neglected. The parasitic capacitance of  $C_2$  is absorbed to  $C_{par}$ . For  $Z_c$  to be regarded as short in node  $X$  and  $Y$  at the desired frequency, the condition  $|Z_c| \ll |Z_t|$  should be met, resulting in a larger capacitance. However,  $C_2$  should be limited in order not to increase the parasitic capacitance  $C_{p,C2}$ . The parasitic capacitance ( $C_{ox}$ ,  $C_{sub}$ ) and substrate loss  $R_{sub}$  of the inductor are considered and can be transformed to a parallel resistor  $R_{p,sub}$  and a capacitor  $C_{p,sub}$ , given by

$$R_{p,sub} \approx \left(1 + \frac{C_{sub}}{C_{ox}}\right)^2 R_{sub} \quad (4.6)$$

$$C_{p,sub} \approx \frac{C_{ox}C_{sub}}{C_{ox} + C_{sub}} \quad (4.7)$$

Inductor  $L_1$  together with the total parasitic capacitance  $C_{par} = C_{p,L1} + C_{p,sub} + C_{p,sw} + C_{p,C2}$  at node  $Y$  is designed to resonate at the desired input signal frequency  $\omega_{RF} = 1/\sqrt{L_1 C_{par}}$ . Regarding the LO waveform as a square wave,

$$sw(t) = \frac{4}{\pi} \left( \sin \omega_{LO} t + \frac{1}{3} \sin 3\omega_{LO} t + \dots \right), \quad (4.8)$$

the conversion gain of the mixer can be expressed as

$$\begin{aligned} G_c &= \frac{2}{\pi} G_{m,eff} (R_L \parallel Z_t) \\ &= \frac{2}{\pi} G_{m,eff} (R_L \parallel R_{p,sub} \parallel R_s (Q^2 + 1)) \end{aligned} \quad (4.9)$$

where  $G_{m,eff} = g_{m1} + g_{m4}$ ,  $R_s$  and  $Q$  are the series resistance and the quality factor of inductor  $L_1$ , respectively. The conversion gain can be made larger with a high- $Q$  inductor, however, high- $Q$  design is more sensitive to parasitics.

The spiral inductors used in the design is a circular spiral inductor with 126- $\mu\text{m}$  inner radius, 5.5 turns, 6- $\mu\text{m}$  width and 2- $\mu\text{m}$  spacing, which occupies quite large area. For practical implementation, the spiral inductor should be optimized to obtain enough  $Q$  while keep the area small. The quality factor in the design is about 7.5 at 2.4 GHz and the 3-dB bandwidth of the impedance  $Z_t$  is about  $f_{RF}/Q \approx 326$  MHz, hence the gain variation in the desired band (83 MHz) is acceptable. Since the conversion gain relates to the inductor  $Q$  value, an accurate model of the inductor is critical. For high- $Q$  designs, a shunt variable capacitor may be added to adjust the resonant frequency. In addition, to overcome the variation of resonant frequency due to ground inductance of bonding wires, a double-balanced topology can be employed with a symmetric spiral inductor whose center tap is connected to ground.

The advantage of the coupling capacitor is twofold. First, the biasing currents of switching stage  $I_{tail}$ , input stage current  $I_{d1}$  as well as injected current  $I_{inj}$  are

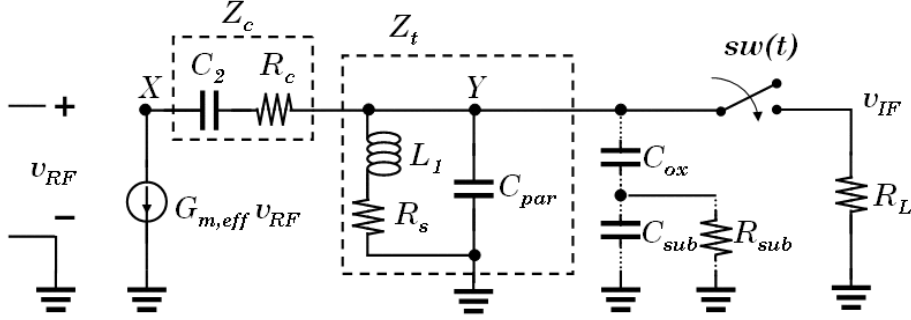
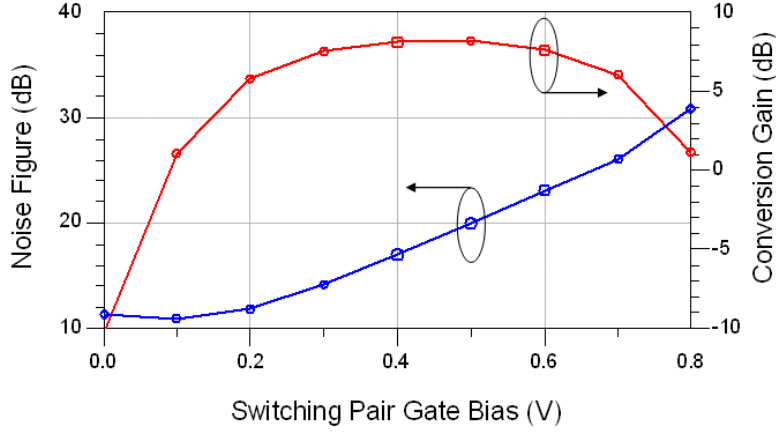


Figure 4.4: Equivalent circuit model for the proposed mixer.


 Figure 4.5: Simulated noise figure and conversion gain of the proposed mixer as the switching pair gate voltage  $V_{LO,BIAS}$  sweep.

separated to decouple the design tradeoff. Second, the capacitor blocks the  $1/f$  noise of the input stage from leaking to output nodes due to mismatched switching pair. Besides the mismatch, the input  $1/f$  noise also leaks to the output in Gilbert-cell and current-injection mixers because of the finite slope of LO waveform at zero crossing that causing a finite duration in which both transistors of the switch pair conduct simultaneously. Increasing the slope of LO waveform reduces the leakage but requires a larger LO power  $P_{LO}$  which consumes more power. Consequently, the  $1/f$  noise of input stage can be substantially blocked only with a capacitor.

Because of AC coupling, the  $1/f$  noise at the mixer output is mainly from the



switching stage, which can be further reduced by modifying the operation region of the switching pair. The input-referred 1/f noise voltage of a MOS transistor in strong inversion and subthreshold regions can be respectively given by [45]

$$S_{V_{g,inv}} \cong \frac{q^2 N_{ot}}{C_{ox}^2 W L f}$$

$$S_{V_{g,sub}} \cong \left[ \frac{C_{inv}}{C_{ox} + C_d + C_{inv}} \right]^2 \frac{q^2 N_{ot}}{C_{ox}^2 W L f} \quad (4.10)$$

where  $N_{ot}$  is the equivalent density of oxide traps,  $C_d$  and  $C_{inv}$  are the depletion and the inversion capacitance, respectively. Since at subthreshold region  $C_{inv} \ll C_{ox} + C_d$ ,  $S_{V_{g,sub}} \ll S_{V_{g,inv}}$  and therefore 1/f noise of the mixer is significantly reduced by operating the switching pair in subthreshold region. Figure 4.5 illustrates the noise figure and conversion gain as a function of gate bias  $V_{LO,BIAS}$  of the switching pair. As  $V_{LO,BIAS}$  decreases, the noise figure becomes lower. If the  $V_{LO,BIAS}$  is set to zero, the noise figure achieves the minimum point because the switching pair operates as a differential voltage switch. Therefore the mixer enters in passive mode and presents significant conversion loss.

Furthermore, the topology also enables low voltage operation, since the switching stage and the input stage are not stacked as the conventional Gilbert-cell topology. Assuming the threshold voltages of  $M_1$  and  $M_4$  are  $V_{th1}$  and  $V_{th4}$ , respectively and the gate overdrive voltages are the same as  $V_{eff}$ , the power supply can be as low as  $|V_{th4}| + V_{th1} + 2V_{eff}$ . Because of the separation of bias currents in V-I conversion and the switching stage, the input third-order intermodulation voltage of the mixer is mainly determined by the input PMOS or NMOS and can be given by

$$V_{IIP3} \approx \min_{(p,n)} \sqrt{\frac{16}{3\Theta}} V_{eff} \quad (4.11)$$

where  $\Theta$  models the mobility degradation and velocity saturation in short channel

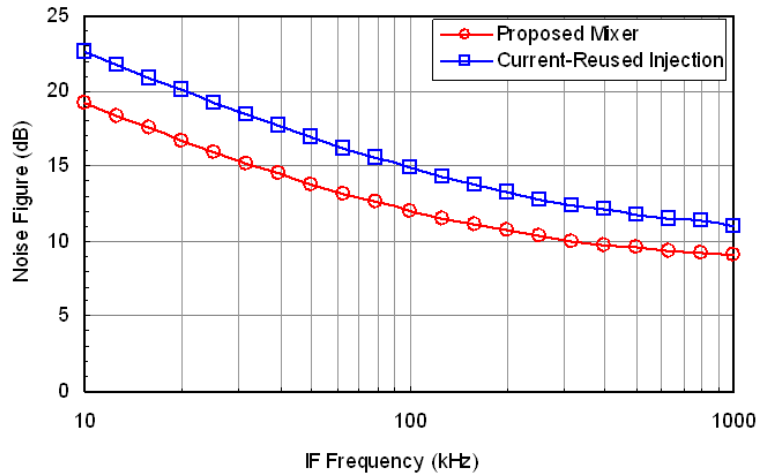


Figure 4.6: Simulated noise figure with IF frequency sweep.

devices. It's apparent that the proposed topology encompass the advantages of current-injection topology while reduces  $1/f$  noise further.

## 4.4 Performance Analysis

A performance comparison is accomplished between the design of 2.4-GHz mixers with both the current-reused injection mixer shown in Figure 4.2 and the proposed folded mixer shown in Figure 4.3. The mixers are intended to be fabricated with 0.18- $\mu\text{m}$  1P6M RFCMOS process which equips with top metal thickness of 2  $\mu\text{m}$  and unit-area MIM capacitance of 1  $f\text{F}/\mu\text{m}^2$  and the device dimensions used in simulation are marked in Figure 4.2 and Figure 4.3. The comparison results of Figure 4.6-4.9 are based on simulations via foundry design kit in which the RF performance of transistors, resistors, spiral inductors and MIM capacitors are well modeled. The  $1/f$  noise model used in the MOS transistors is BSIM3v3 instead of SPICE2 model to provide more accurate prediction in the bias region of the switching pair [46]. Since the  $1/f$  noise dominates low frequency noise of direct conversion mixers, the intermediate frequency selection affects the noise figure results. Figure 4.6 depicts the noise figure as a function of intermediate frequency

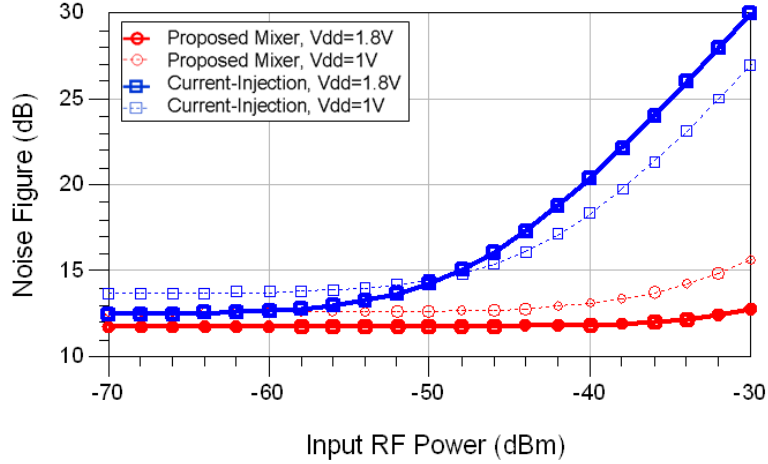


Figure 4.7: Simulated noise figure with RF input power sweep.

Table 4.1: Comparison of the current-reused injection mixer and the proposed current-folded mixer performances based on simulations.

| Specifications<br>$f_{RF}=2.4\text{GHz}$ , $P_{LO}=0\text{dBm}$ | NF<br>[dB] | Gain<br>[dB] | IIP3<br>[dBm] | $I_{inj}$<br>[ $\mu\text{A}$ ] | $I_{DC}$<br>[ $\mu\text{A}$ ] | $f_{IF}$<br>[MHz] | FOM<br>[dB] |
|---|------------|--------------|---------------|--------------------------------|-------------------------------|-------------------|-------------|
| Proposed mixer @ 1.8V   | 11.77      | 5.76         | -7.36         | 593                            | 594                           | 0.23              | 16.64       |
| Proposed mixer @ 1V   | 12.60      | 3.18         | -6.48         | 498                            | 499                           | 0.23              | 17.38       |
| Figure 4.2 @ 1.8V   | 12.50      | -1.46        | -16.08        | 593                            | 594                           | 0.23              | -0.07       |
| Figure 4.2 @ 1V   | 13.70      | -2.99        | -15.67        | 498                            | 499                           | 0.23              | 0.86        |
| Figure 4.2 @ $V_{LO,BIAS} = 1.5\text{V}$                        | 13.64      | 6.24         | -11.45        | 576                            | 640                           | 0.23              | 10.73       |
| Ref [44], $f_{RF}=900\text{MHz}$                                | 11.20      | 4.00         | -5.60         | 2000                           | 4000                          | 100.00            | 2.34        |

when input RF frequency is fixed at 2.4 GHz. The noise figure of the proposed mixer is lower than that of the current-reused injection mixer because of the less  $1/f$  noise contribution of the input stage to the output.

To characterize the mixer performance as RF input power sweeps, the IF frequency is chosen as 230 kHz in the following comparisons. In addition, the bias currents of the two mixers are set the same around  $594 \mu\text{A}$  at 1.8 V and  $499 \mu\text{A}$  at 1 V. The noise figure and *voltage* conversion gain results of both mixers are shown in Figure 4.7 and Figure 4.8. The conversion gain of the proposed mixer is about 6 dB better than that of the current-reused injection mixer while noise figure is about

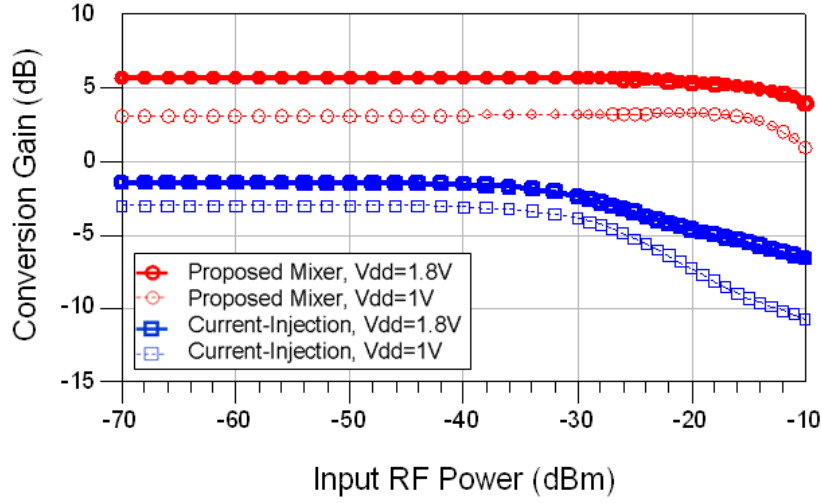


Figure 4.8: Simulated conversion gain with RF input power sweep.

1 dB lower. The current-reused injection mixer has not only worse noise figure and conversion gain performance but also the worst intermodulation distortion. As a result, the noise figure of current-reused injection mixer increases rapidly as input RF power is larger than  $-50$  dBm, while the noise figure of the proposed mixer increases slowly even when in RF power is larger than  $-30$  dBm.

To show the intermodulation distortion of both mixers, the parameter IM3 is employed in Figure 4.9, which is the ratio of magnitude of the third order intermodulation term to that of the fundamental term. IM3 reveals how much intermodulation distortion of each mixer would produce. The current-reused injection mixer produces more intermodulation distortion than the proposed mixer.

A figure of merit (FOM) which normalizes dynamic range to power dissipation is employed to compare the performance of the mixers:

$$FOM_{dB} \equiv 10 \log \left( \frac{IIP3(mW) \cdot Gain}{(NF - 1) \cdot V_{DD} \cdot I_{DC}} \right) \quad (4.12)$$

Table 4.1 summarizes the simulation results of the mixers. The proposed current-folded mixer demonstrates about 1-dB lower noise figure, about 6-dB higher

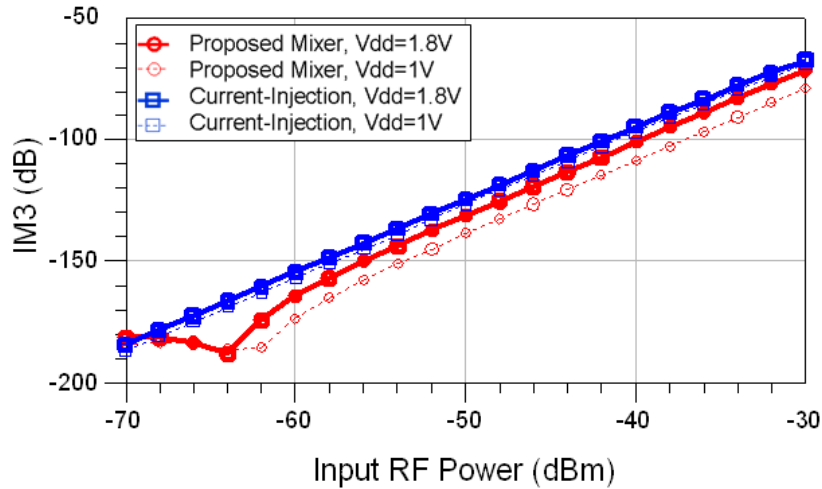


Figure 4.9: Simulated IM3 with RF input power sweep.

conversion gain and about 9-dB higher IIP3, which is 16-dB more improvement in FOM. The proposed mixer consumes 1.07 mW and 0.5 mW at 1.8 V and 1 V supplies, respectively and is suitable for low power RF applications. The proposed current-folded mixer shows superiority to the current-reused injection mixer in FOM because of the limited switching-pair current in current-reused injection topology, which is in order to keep the same power consumption and to assure the switching stages in both mixers are biased in subthreshold region. Since the switching pair of current-injection mixer is DC coupled to the input stage, such gate bias condition forces the drain-source voltage of the input stage to be lower. Hence the intermodulation performance is seriously affected. Increasing the switching pair current ( $V_{LO,BIAS}=1.5$  V) of the current-reused injection mixer improves the gain and linearity performance but the cost is worse noise figure and larger power consumption (1.15 mW) as shown in Table 4.1.

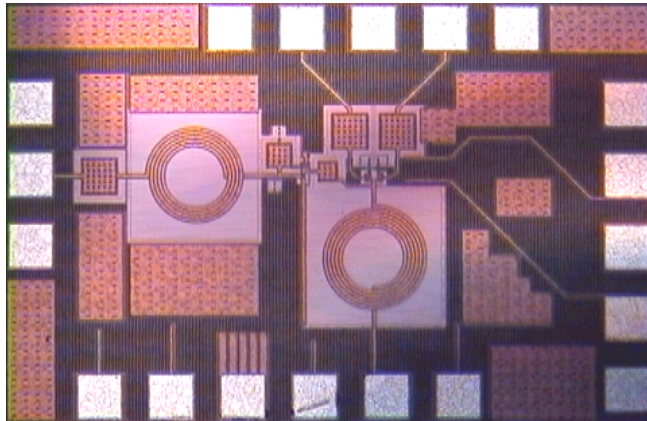


Figure 4.10: The proposed current-folded mixer chip photograph.

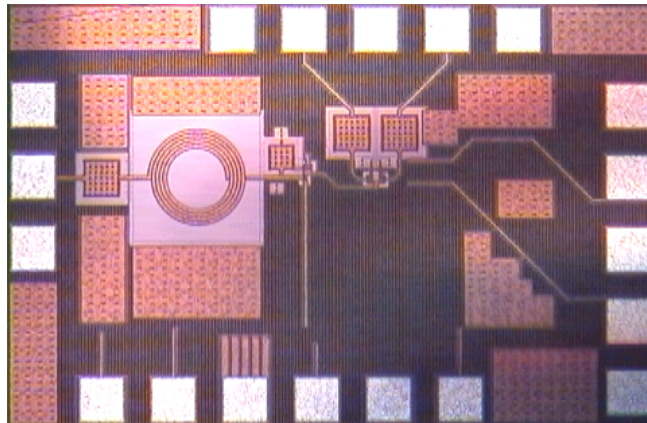


Figure 4.11: Current-reused injection mixer chip photograph.

## 4.5 Experimental Results

Both the mixers are fabricated and configured to be measured on wafer level. At the interface between the mixer output port and the instrument, a output source-follower buffer is added to convert the output impedance of the mixer to avoid the loading effect of the instrument. To overcome the loss due to the buffer,  $R_L$  is increased to 2 K $\Omega$ . The chip photos are shown in Figure 4.10 and Figure 4.11. The conversion gain hereafter are referred to power gain, since the input and output impedance are the same as 50  $\Omega$ .

The IF should be as low as possible to characterize the effect of flicker noise on

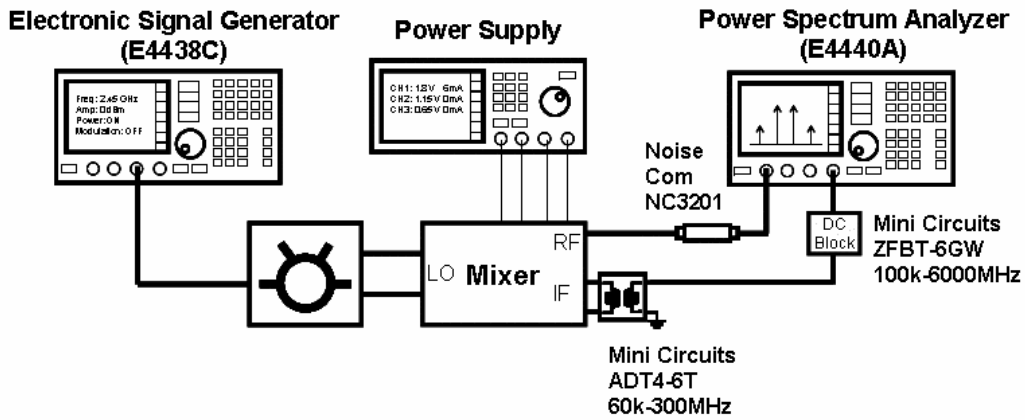


Figure 4.12: Noise figure measurement setup.

noise figure, however, the minimum frequency allowable for the noise figure meter is 10 MHz. Instead of using a noise figure meter, the noise figure measurement is performed with an power spectrum analyzer (PSA, Agilent E4440A) and an ENR (Excess Noise Ratio) source NC3201. The noise figure measurement setup is illustrated in Figure 4.12. A rat-race coupler is used as a balun to convert the LO signal to differential signals. A transformer is adopted as differential-to-single converter at IF port. Though the spectrum analyzer is configured to have DC coupled input to measured the low IF frequencies, a bias-tee (100 kHz-6000 MHz) is insert to protect the analyzer. Both 1.8 V and 1.2 V power supply voltages are considered in the following measurements. When low-voltage mode, the power supply for all circuits is reduced to 1.2 V, while keeping the gate over-drive voltage of the input stage the same as in high voltage mode. Since the switching pair consumes little current and the input stage consumes about  $500 \mu\text{A}$ , most of the current change in low-voltage mode comes from the output buffer.

The measured noise figure performance of both mixers are shown in Figure 4.13. The measurement condition is that LO frequency is fixed at 2.45 GHz as the RF frequency sweeps and hence the IF frequency sweeps. Owing to the ENR frequency limitation, the lowest IF frequency can be measured is 1 MHz, which is the lower



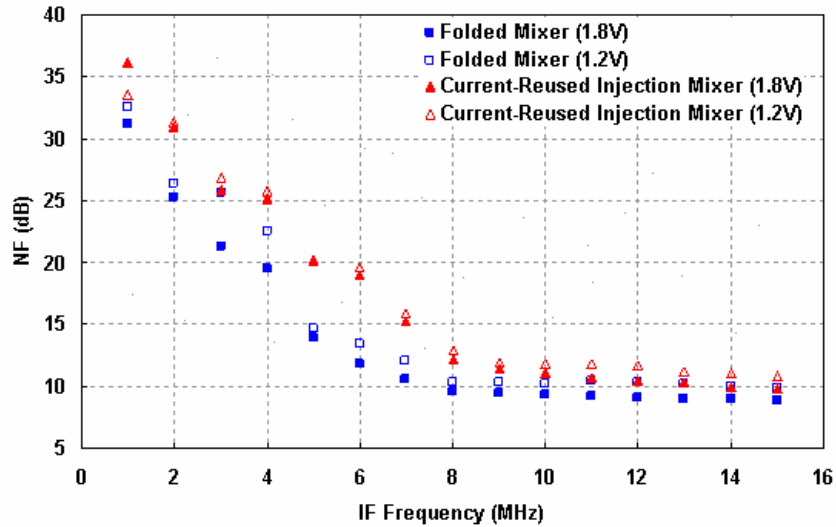


Figure 4.13: Measured noise figure.

end of the ENR and the result at the point is not accurate. The noise figure of the proposed mixer indeed is lower than that of the current-reused injection mixer, especially at very low IF frequency, demonstrating the flicker noise reduction ability of the proposed topology. Even at low-voltage mode ( $V_{dd}=1.2$  V), the noise figure of the proposed mixer is still lower than that of the current-reused injection mixer. Figure 4.14 depicts the measured *power* conversion gain as the RF frequency sweep with the LO is fixed at 2.45 GHz. The conversion gain of the proposed mixer is larger than the current-reused injection mixer as the simulation predicts.

The noise figure and conversion gain vary with LO power levels and the measurement results are depicted in Figure 4.15 and Figure 4.16. As the LO power increases, the noise figure decreases and the conversion gain increases. The conversion gain and noise figure saturates at LO power level of 0 dBm.

The bias voltage of the switching pair affects the most of  $1/f$  noise contribution. If the switching pair bias at the optimum point, the noise figure can be lowered. The noise figure and conversion gain of both mixers as the gate bias voltage of the switching pairs sweeps are measured and Figure 4.17 and Figure 4.18. The gate



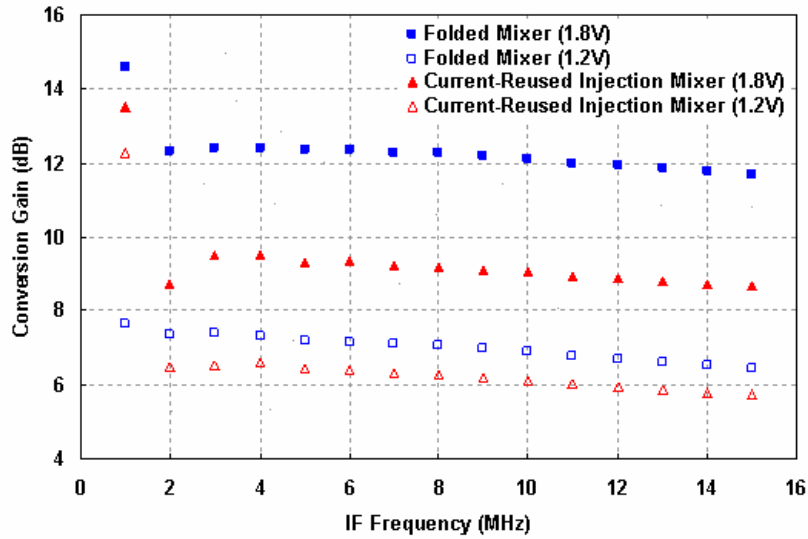


Figure 4.14: Measured conversion gain.

bias switching pair indeed plays an important role on the  $1/f$  noise of the proposed mixer. As the voltage increases, the  $1/f$  noise of the switching gate increases and so does noise figure. In addition, the mixer has a source follower appended at the switching pair output, as the bias point further increases, the gate voltage of the source follower decreases and gradually shuts off the buffer, resulting in decrease of the conversion gain.

The intermodulation measurement is performed by input a 2.45 GHz as LO signal and 2.455 GHz and 2.457 GHz as the two-tone input RF signals. The IF frequency is 5 MHz, the IM2 term is located at 2 MHz and the IM3 term is located at 9 MHz. The measured IM2 and IM3 of the proposed mixer at 1.8 V and 1.2 V are shown in Figure 4.19 and Figure 4.20. The measured IM2 and IM3 of the current-reused injection mixer are shown in Figure 4.21 and Figure 4.22. The input IP3 and IP2 of the proposed folded mixer are much better than those of the current-reused injection mixer in high voltage mode (1.8 V power supply). The IP3 and IP2 of the proposed mixer is degraded when 1.2 V supply voltage is applied, which comes from the serious degradation of the buffer current compared with the current-reused injection mixer.

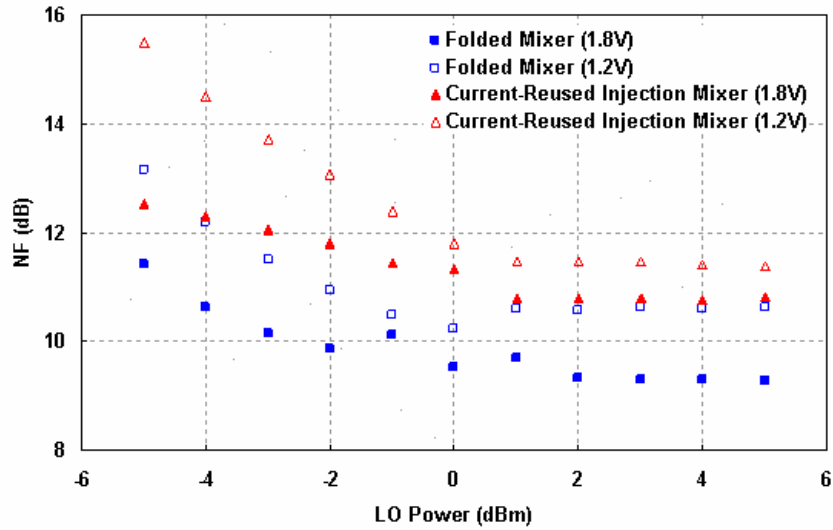


Figure 4.15: Measured noise figure as LO power level sweeps.

The linearity of the current-reused injection mixer is limited by the shared current of input driver stage and the switching stage and hence the IP3 is worse. The proposed mixer exhibits better IP3 performance than the current-reused injection mixer. As for IP2, the folded mixer shows higher input IP2 than the reused injection mixer at high voltage mode.

The buffer is not necessary if an AC coupled highpass filter is inserted in the mixer output, which is the case in integrated direct conversion receivers. Hence the  $1/f$  noise of the switching mixer in the proposed mixer is not so sensitive to the gate bias as the case with buffers. The current consumption of both mixers is about 7 mA. The mixer core consumes current as little as 0.5 mA and the buffer drains most of the current about 6.5 mA. Table 4.2 summarizes the performances of both mixers.

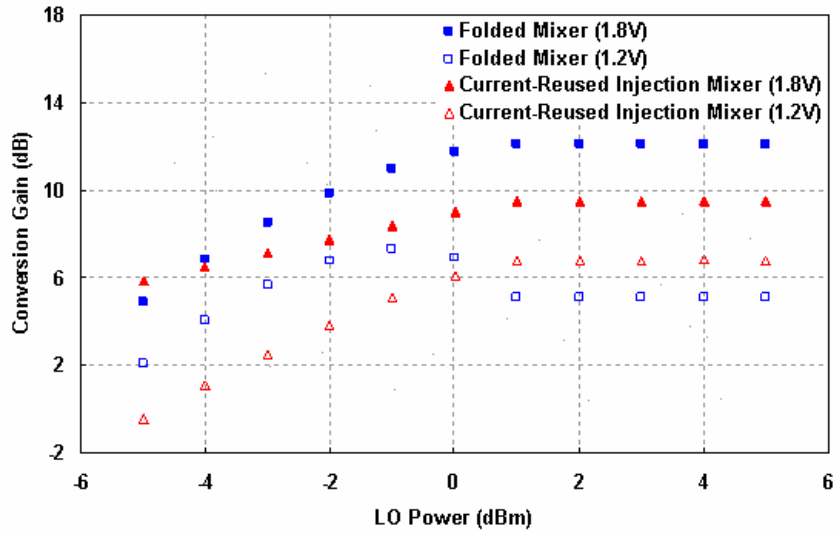


Figure 4.16: Measured conversion gain as LO power level sweeps.

Table 4.2: Performance summary of both mixers

| Mixers                         | NF [dB] | CG [dB] | IIP3 [dBm] | IIP2 [dBm] | $I_D$ [mA] | $f_{IF}$ [MHz] | FOM [dB] |
|--------------------------------|---------|---------|------------|------------|------------|----------------|----------|
| Proposed Mixer @ 1.8 V         | 11.76   | 13.16   | -4.17      | 10.18      | 7.10       | 5.0            | 16.46    |
| Proposed Mixer @ 1.2 V         | 13.40   | 7.21    | -9.91      | -5.16      | 4.24       | 5.0            | 5.28     |
| Reused Injection Mixer @ 1.8 V | 18.99   | 9.51    | -11.90     | 0.95       | 6.72       | 5.0            | -2.14    |
| Reused Injection Mixer @ 1.2 V | 19.56   | 6.86    | -12.07     | -1.39      | 6.04       | 5.0            | -5.08    |

## 4.6 Summary

A current-folded mixer topology, which uses a capacitor to separate the bias current of input stage and switching stage and employs an inductor to replace tail current source of the switching pair is proposed. The mixer decouples the noise and linearity design tradeoff and exhibits higher conversion gain, higher linearity and lower noise figure than conventional current-reused injection topology. A 2.4-GHz single-balanced current-folded mixer has been designed as an example to demonstrate significant performance improvements.

#### 4.6. SUMMARY

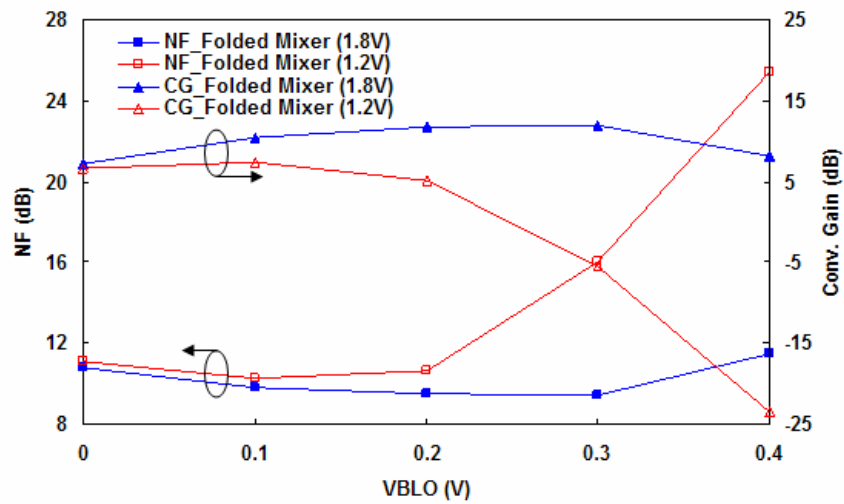


Figure 4.17: Measured noise figure and conversion gain of the proposed mixer as  $V_{B,LO}$  sweeps.

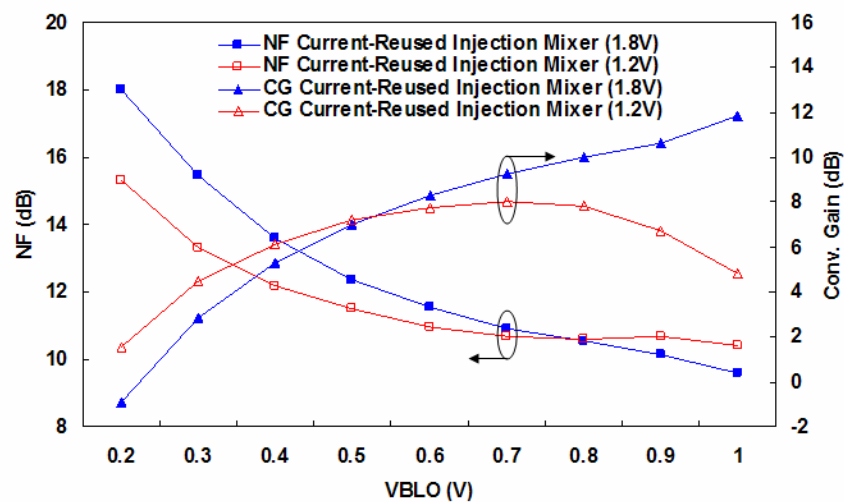


Figure 4.18: Measured noise figure and conversion gain of the current-reused injection mixer as  $V_{B,LO}$  sweeps.

#### 4.6. SUMMARY

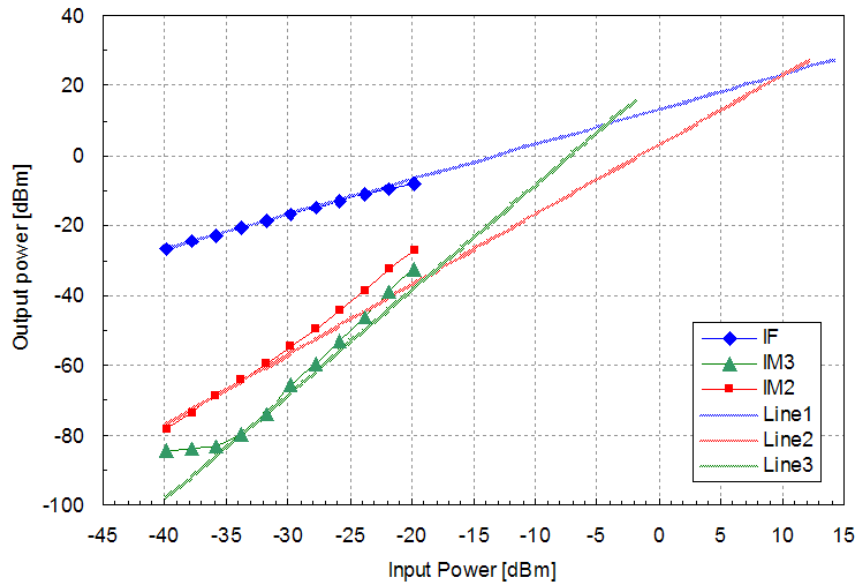


Figure 4.19: Measured 2<sup>nd</sup> and 3<sup>rd</sup> order intermodulation of the proposed mixer at 1.8V power supply.

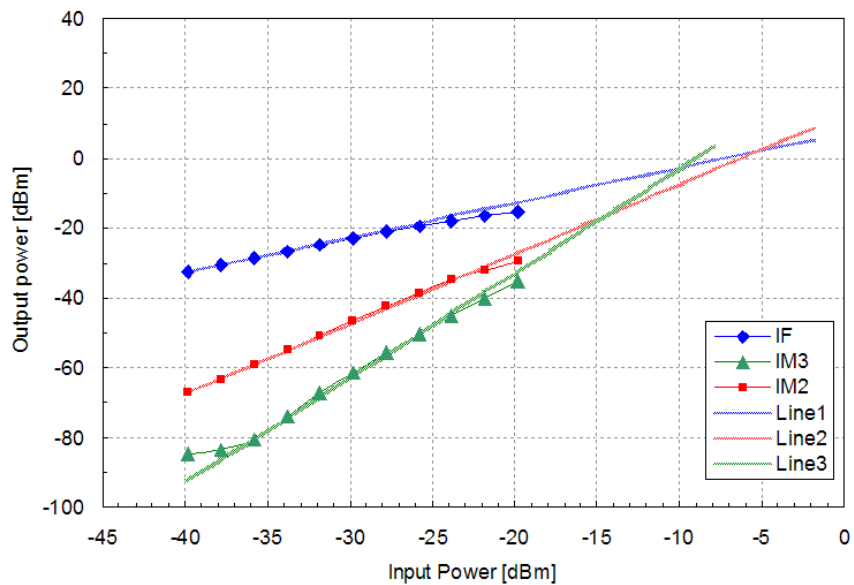


Figure 4.20: Measured 2<sup>nd</sup> and 3<sup>rd</sup> order intermodulation of the proposed mixer at 1.2V power supply.

#### 4.6. SUMMARY

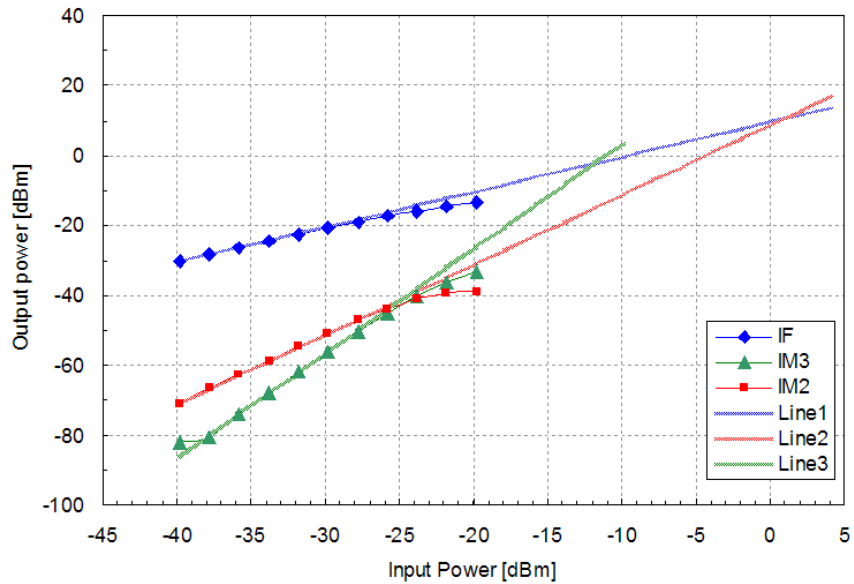


Figure 4.21: Measured 2<sup>nd</sup> and 3<sup>rd</sup> order intermodulation of the current-reused injection mixer at 1.8V power supply.

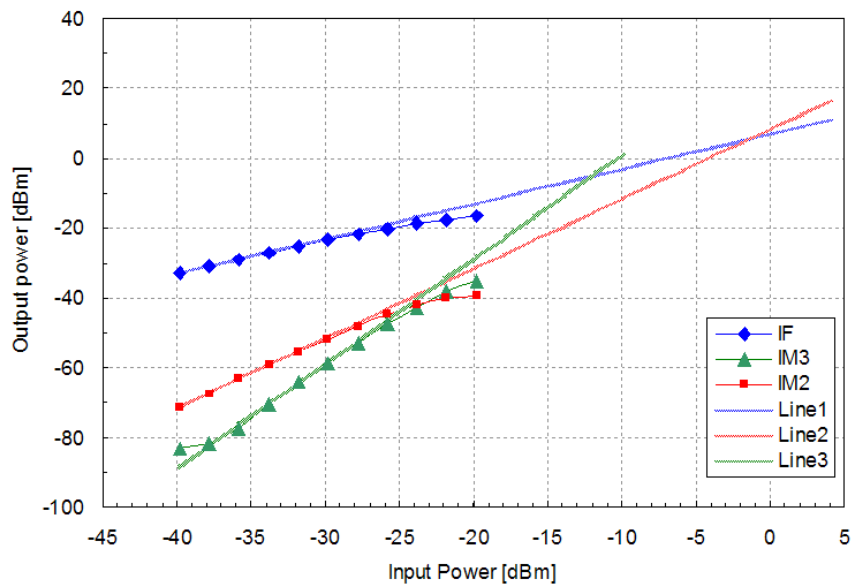


Figure 4.22: Measured 2<sup>nd</sup> and 3<sup>rd</sup> order intermodulation of the current-reused injection mixer at 1.2V power supply.